Crystal and Magnetic Structure of the Orthorhombic Perovskite $YbMnO_3$

Y. H. Huang,[†,‡] H. Fjellvåg,[§] M. Karppinen,*[,†,||] B. C. Hauback,[⊥] H. Yamauchi,[†] and J. B. Goodenough[‡]

Materials and Structures Laboratory, Tokyo Institute of Technology, Yokohama 226-8503, Japan, Centre for Materials Science and Nanotechnology, Department of Chemistry, University of Oslo, Blindern N-0315 Oslo, Norway, Laboratory of Inorganic and Analytical Chemistry, Helsinki University of Technology, FI-02150 Espoo, Finland, Institute for Energy Technology, N-2027 Kjeller, Norway, and Texas Materials Institute, ETC 9.102, The University of Texas at Austin, Austin, Texas 78712

Received December 14, 2005. Revised Manuscript Received February 21, 2006

The perovskite polymorph of $YbMnO_3$ has been revisited. The orthorhombic phase is obtained through a high-pressure (HP) reconstructive transformation from the hexagonal sol−gel-synthesized $YbMnO_3$ by means of HP annealing at 5 GPa and 1100 °C. Neutron powder diffraction shows that the HP form crystallizes in the orthorhombic space group *Pbnm*. At 298 K, the refined values for lattice parameters *a*, *b*, and *c* are respectively 5.2208(3), 5.8033(3), and 7.3053(4) Å. The average Mn−O−Mn angle is 141.9°, indicative of a strong tilting of the MnO_6 octahedra. Magnetic susceptibility measurements indicate antiferromagnetic order of Mn^{3+} spins at $T_N = 43$ K and of Yb^{3+} spins at 4 K. The magnetic structure is commensurate A_y with an ordered moment 3.45(5) μ_B at 9 K. The magnetic susceptibility obeys the Curie−Weiss law, $\chi = C/(T - \theta)$, in two temperature regions, that is, above 240 K and 6−30 K. The obtained effective paramagnetic moments μ_{eff} are 6.37 μ_B and 4.83 μ_B for the two temperature ranges, respectively. The former is attributed to a superposition of paramagnetic Mn^{3+} and Yb^{3+} spins while the latter reflects primarily the paramagnetic Yb^{3+} moments. Re-entry of A_y magnetic ordering requires a reconsideration of the factors that contribute to the competitive spin−spin interactions on the MnO_3 array.

Introduction

The $RMnO_3$ family has the orthorhombic (space group *Pbnm*) perovskite structure for the larger rare-earth atoms R = La−Dy and a noncentrosymmetric hexagonal structure (space group $P6_3cm$) for the smaller rare earths (R = Ho−Lu, Y and Sc).[1,2] However, the hexagonal compounds can all be synthesized under high pressure as a metastable orthorhombic perovskite.[3] The R = Y, Ho, and Er compounds have also been synthesized as perovskites by a low-temperature soft-chemistry route[4,5] or as an epitaxial thin film.[6]

Figure 1 shows the phase diagram for the perovskite structures.[7] Magnetization $M(T)$ below T_N distinguishes the weak, canted-spin ferromagnetic behavior of compounds with R = La−Gd (group I) from that of compounds with R = Y, Ho−Lu (group II). The antiferromagnetic (AFM) order below T_N of all the group I compounds consists of ferromagnetic (001) planes coupled antiparallel to one another with a canted-spin ferromagnetic component along the *Pbnm* *b* axis (type A_y). The spin ordering of the group II compounds has not yet been fully characterized. Different neutron-diffraction studies[8,9] have described the AFM order of the

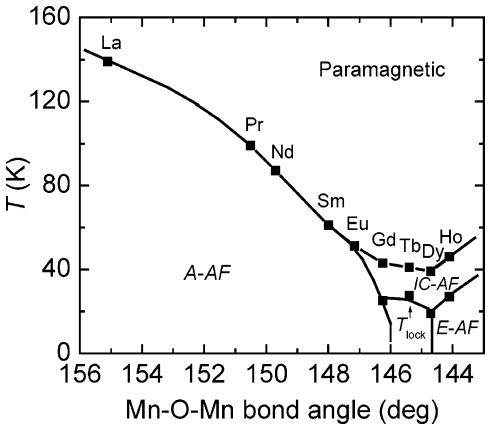

Figure 1. Phase diagram of $RMnO_3$ with the orthorhombic perovskite structure from ref 7.

* Corresponding author. Phone: +81-45-924-5333. Fax: +81-45-924-5365. E-mail: karppinen@msl.titech.ac.jp.
[†] Tokyo Institute of Technology.
[‡] The University of Texas at Austin.
[§] University of Oslo.
[||] Helsinki University of Technology.
[⊥] Institute for Energy Technology.

(1) Yakel, H. L. *Acta Crystallogr.* **1955**, *8*, 394.
(2) Yakel, H. L.; Koehler, W. C.; Bertaut, E. F.; Forrat, E. F. *Acta Crystallogr.* **1963**, *16*, 957.
(3) Waintal, A.; Capponi, J. J.; Bertaut, E. F.; Contré, M.; Francois, D. *Solid State Commun.* **1966**, *4*, 125. Waintal A.; Chevanas, J. *Mater. Res. Bull.* **1967**, *2*, 819.
(4) Quezel, S.; Mignod, J. R.; Bertaut, E. F. *Solid State Commun.* **1974**, *14*, 941.
(5) Brinks, H. W.; Fjellvåg, H.; Kjekshus, A. *J. Solid State Chem.* **1997**, *129*, 334.
(6) Salvador, P. A.; Doan, T.-D.; Mercey, B.; Raveau, B. *Chem. Mater.* **1998**, *10*, 2592.
(7) Kimura, T.; Ishihara, S.; Shintani, H.; Arima, T.; Takahashi, K. T.; Ishizaka, K.; Tokura, Y. *Phys. Rev. B* **2003**, *68*, 60403R.

10.1021/cm052758t CCC: $33.50
Published on Web 03/28/2006

MnO_3 array in terms of type *E* or sinusoidally modulated type A_y spin structures. A type *E* magnetic order is assumed for all the group II compounds in the phase diagram of Figure 1, but further clarification of the magnetic order is needed. For R = Ho, incommensurate ordering of both Mn and Ho spins occurs, at low temperatures accompanied by a minority commensurate AF phase.[8] The type *E* AFM order consists of [110] rows of spins coupling parallel to a neighboring row on one side and antiparallel on the other with antiparallel coupling between (001) planes. This order suggests that the competition between ferromagnetic coupling by σ-bonding *e* electrons and AFM coupling by π-bonding *t* electrons in the (001) planes has come into a balance that is resolved by stabilization of a spin-density wave. The spin configurations of the transitional $TbMnO_3$ and $DyMnO_3$ perovskites are sinusoidally modulated with a transition from incommensurate to commensurate wavelength below T_{lock}.[7] The complex magnetic order found for the transitional and group II compounds has been discussed in terms of frustration between competing nearest-neighbor and next-nearest-neighbor interactions.[7]

Although all the group II perovskites were first synthesized under pressure decades ago,[3] the structures of most of the $RMnO_3$ perovskites have only recently been characterized with neutron diffraction.[10] The present work reports a neutron powder diffraction (NPD) and magnetic study of orthorhombic o-$YbMnO_3$, a phase last studied magnetically by Wood et al.[11] in 1973. The observation of a type A_y magnetic order at 9 K implies that the evolution of the competitive interatomic interactions become reversed as the radius of the R^{3+} ion is further reduced.

Experimental Section

A high-quality sample of o-$YbMnO_3$ was obtained through high-pressure (HP) annealing of single-phase powder of the hexagonal polymorph. This starting material was synthesized through a wet-chemical route utilizing ethylenediaminetetraacetic acid (EDTA) as a complexing agent. Stoichiometric amounts of Yb_2O_3 and $MnCO_3$ were first dissolved in a diluted nitric acid. This solution was added stepwise to an NH_4−EDTA solution while stirring at ambient temperature. A clear solution was obtained, and the pH was adjusted to ∼9. The molar ratio between EDTA and metal ions was 1.5. During heating at ∼200 °C, an amorphous gel was formed. The gel ignited spontaneously upon further water evaporation. The ash was calcined in air at 800 °C for 8 h and then fired at 1200 °C for 20 h. The thus prepared powder of hexagonal h-$YbMnO_3$ was packed into a gold capsule and treated in a cubic-anvil-type HP apparatus (at Tokyo Tech) at 5 GPa and 1100 °C for 30 min.

The samples were characterized by room-temperature X-ray powder diffraction (XRD) measurements (Rigaku, RINT2550VK/U; Cu K_α radiation) for phase purity and lattice parameter determinations. Atomic and magnetic structure parameters were determined by NPD at the JEEP-II reactor at Kjeller, Norway, with the high-resolution two-axis powder diffractometer, PUS. The sample (∼0.4 g) was packed in a cylindrical vanadium sample holder and sealed with an indium washer. Monochromatized neutrons of wavelength 1.5554 Å were obtained from a Ge(511) monochromator. A total of 2400 data points were collected in the 2θ range of 10−130° (in 2θ steps of 0.05°) by means of two detector units, and each unit contained a vertical stack of seven position-sensitive ^{3}He detectors covering a range of 20° in 2θ. A Displex cooling system was used for the low-temperature measurements. The structure refinements were made with the GSAS and FULLPROF softwares. Regions with scattering from Al of the cryostat were excluded. Corrections were done for an instrumental peak at $2\theta = 32°$. The data were fitted with a Gaussian peak shaped function. Isotropic displacement factors were refined for each of the three types of atoms, Yb, Mn, and O. Micrographs of the samples were taken with a scanning electron microscope (SEM; Hitachi, S4500). Magnetization measurements were performed on a superconducting quantum interference device (SQUID) magnetometer (Quantum Design, MPMS-XL5).

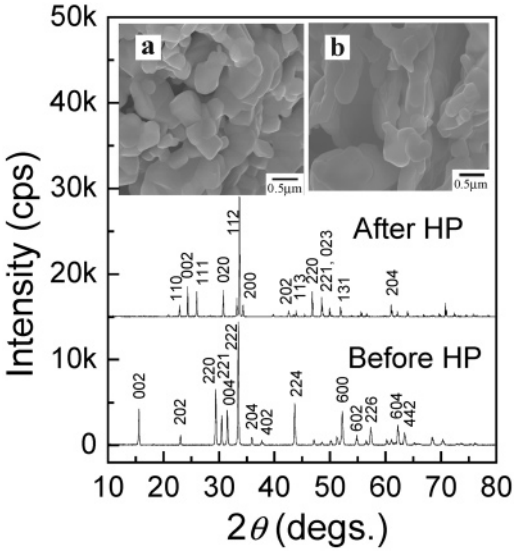

Figure 2. XRD patterns and SEM images for $YbMnO_3$ (a) before (hexagonal) and (b) after (orthorhombic) HP heat treatment.

Results and Discussion

Figure 2 shows XRD patterns and SEM images for $YbMnO_3$ before and after HP annealing. The air-synthesized sample (without HP treatment) presents the pure hexagonal h-$YbMnO_3$ phase. Rietveld refinement in space group $P6_3cm$ gave the lattice parameters $a = 6.0682(3)$ Å and $c = 11.3533(4)$ Å, which are in good agreement with those previously reported.[12,13] The HP-annealed sample exhibits a completely different XRD pattern that is perfectly compatible with those for orthorhombic $RMnO_3$ perovskites with space group *Pbnm*. It was checked that the HP treatment alone, that is, without any heating, does not give the orthorhombic phase, which indicates that heating is required for nucleation and formation of the HP phase. The SEM images in Figure 2 show that there is no major change in the grain size (∼300 nm) upon HP annealing. The main observable difference in

(8) Brinks, H. W.; Rodríguez-Carvajal, J.; Fjellvåg, H.; Kjekshus, A.; Hauback, B. C. *Phys. Rev. B* **2001**, *63*, 094411.
(9) Muñoz, A.; Casáis, M. T.; Alonso, J. A.; Martínez-Lope, M. J.; Martínez, J. L.; Fernández-Díaz, M. T. *Inorg. Chem.* **2001**, *40*, 1020.
(10) Alonso, J. A.; Martínez-Lope, M. J.; Casáis, M. T.; Fernández-Díaz, M. T. *Inorg. Chem.* **2000**, *39*, 917.
(11) Wood, V. E.; Austin, A. E.; Collins, E. W.; Brog, K. C. *J. Phys. Chem. Solids* **1973**, *34*, 859.
(12) Isobe, M.; Kimizuka, N.; Nakamura, M.; Mohri, T. *Acta Crystallogr., Sect. C* **1991**, *47*, 423.
(13) Van Aken, B. B.; Meetsma, A.; Palstra, T. T. M. *Acta Crystallogr., Sect. E* **2001**, *57*, i87.

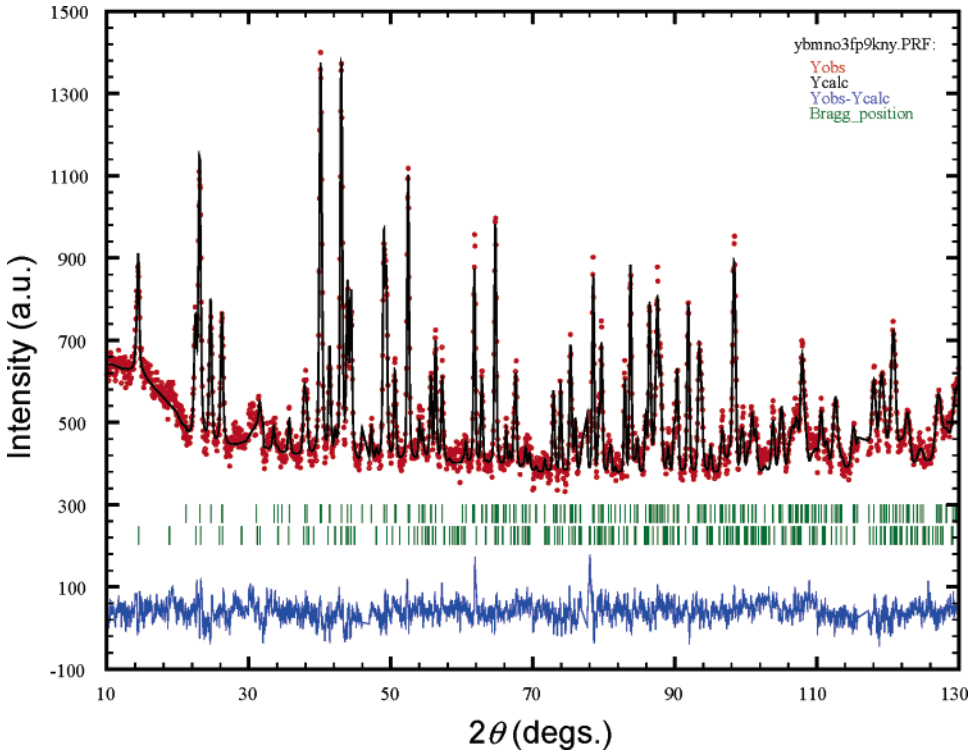

Figure 3. Observed, calculated, and difference NPD profiles from Rietveld refinement of data for orthorhombic $YbMnO_3$ at 9 K. Upper ticks refer to Bragg positions for the nuclear structure; lower ticks refer to magnetic reflections. The very first reflection is the most prominent (001) magnetic reflection mentioned in the text.

morphology between the samples before and after HP annealing is an enhanced grain aggregation after the HP annealing.

Crystallographic details for o-$YbMnO_3$ were derived from a Rietveld refinement of the NPD data. Observed, calculated, and difference NPD intensity profiles are shown in Figure 3. Lattice parameters and atomic positions are given in Table 1. At 298 K, the calculated lattice parameters are $a = 5.2208(3)$ Å , $b = 5.8033(3)$ Å, and $c = 7.3053(4)$ Å. These values agree well with the order $c/\sqrt{2} < a < b$, which is consistent with orbital ordering and distortion of the MnO_6 octahedra due to a strong cooperative Jahn−Teller effect.[8] The Jahn−Teller deformation is clearly evident in the Mn−O bond lengths (Table 1). The influence of the size of the R^{3+} cations on structural properties is illustrated and compared for the o-$RMnO_3$ compounds in Figure 4 (data from refs 8, 10, and 14). The Goldschmidt tolerance factor is $t \equiv (r_R + r_O)/\sqrt{2}(r_{Mn} + r_O)$, where r_R, r_{Mn}, and r_O represent the ionic radii[15] for R^{3+}, Mn^{3+}, and O^{2-}, respectively. The values used were those with CN = 9 for R^{3+} and CN = 6 for Mn^{3+}; t varies strongly with the R^{3+} size. For o-$YbMnO_3$, t is as low as 0.848. With decreasing t (i.e., decreasing ionic radius of R^{3+}), lattice parameters a and c, unit-cell volume V, average bond length ⟨R−O⟩ of the eight shortest bonds, and average bond angle ⟨Mn−O−Mn⟩ are seen to decrease monotonically, whereas the b-axis length and the average ⟨Mn−O⟩ bond length remain essentially unchanged. Throughout the R series, the 4+2 coordination for Mn^{3+} is retained, but the average ⟨Mn−O−Mn⟩ bond angle decreases from ∼155 to ∼142° as R varies from La to Yb. This reflects enhanced octahedral tilting for small R. Thus, the crystal structure of o-$YbMnO_3$ is strongly distorted.

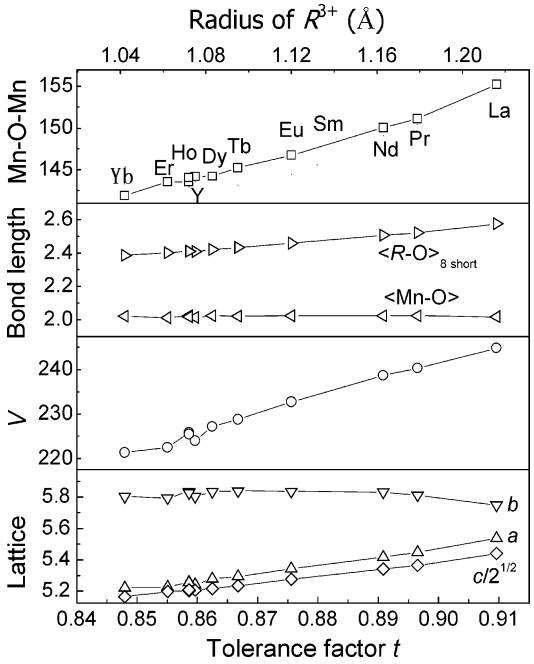

Figure 4. Effects of tolerance factor (t) as well as radii of rare-earth ions at the A site on lattice parameters a, b, and $c/\sqrt{2}$ (Å), unit-cell volume V (Å^3), average bond length ⟨Mn−O⟩ and ⟨R−O⟩ for eight short bonds (Å), and average bond angle ⟨Mn−O−Mn⟩ (deg) for orthorhombic $RMnO_3$. All the data are obtained from neutron diffraction at room temperature. The data for most $RMnO_3$ are from ref 10 except for R = Eu (ref 14), Ho (ref 8 for comparison), and Yb (the present work). To our knowledge, there are no neutron data reported for R = Sm, Gd, Tm, and Lu.

Figure 5 presents the inverse magnetic susceptibility (χ^{-1}) for h- and o-$YbMnO_3$ with respect to temperature. For both

(14) Dabrowski, B.; Kolesnik, S.; Baszczuk, A.; Chmaissem, O.; Maxwell, T.; Mais, J. *J. Solid State Chem.* **2005**, *178*, 629.
(15) Shannon, R. D. *Acta Crystallogr., Sect. A* **1976**, *32*, 751.

Table 1. Unit Cell Dimensions, Atomic Coordinates, Isotropic Displacement Factors, and Reliability Factors from Rietveld Refinement NPD Data at 9 and 298 K for Orthorhombic $YbMnO_3$, Space Group *Pbnm*, $Z = 4$[a]

		9 K	298 K
a (Å)		5.2160(3)	5.2208(3)
b (Å)		5.8030(3)	5.8033(3)
c (Å)		7.2816(4)	7.3053(4)
V (Å^3)		220.40(2)	221.33(2)
Yb	4c(x y $^1/_4$)		
x		0.9826(7)	0.9836(7)
y		0.0851(5)	0.0856(5)
B (Å^2)		0.21(7)	0.27(8)
Mn	4b($^1/_2$ 0 0)		
B (Å^2)		0.80(17)	0.74(23)
O1	4c(x y $^1/_4$)		
x		0.1187(12)	0.1183(11)
y		0.4558(11)	0.4572(11)
B (Å^2)		0.33(9)	0.25(10)
O2	8d(x y z)		
x		0.6970(8)	0.6993(8)
y		0.3310(8)	0.3306(8)
z		0.0548(6)	0.0557(6)
B (Å^2)		0.33(9)	0.25(10)
		MnO_6 octahedra	
Mn−O1−Mn (deg)	×2	139.579	139.947
Mn−O2−Mn (deg)	×4	142.638	142.806
⟨Mn−O−Mn⟩ (deg)		141.618	141.853
Mn−O1 (Å)	×2	1.9398	1.9439
Mn−O2 (Å)	×2	1.9023	1.8965
Mn−O2 (Å)	×2	2.2146	2.2202
⟨Mn−O⟩ (Å)		2.0189	2.0202
		YbO_9 polyhedra	
Yb−O1 (Å)	(long) ×1	3.2249	3.2295
Yb−O1 (Å)	×1	2.2108	2.2079
Yb−O1 (Å)	×1	2.2653	2.2683
Yb−O2 (Å)	×2	2.5051	2.4979
Yb−O2 (Å)	×2	2.2522	2.2620
Yb−O2 (Å)	×2	2.5325	2.5479
⟨Yb−O⟩ (Å)	(8 short)	2.3820	2.3865
R_p (%)		3.9	4.6
R_{wp} (%)		5.0	5.7
χ^2		1.31	1.15
R_{magn} (%)		10.1	

[a] Calculated standard deviations in parentheses.

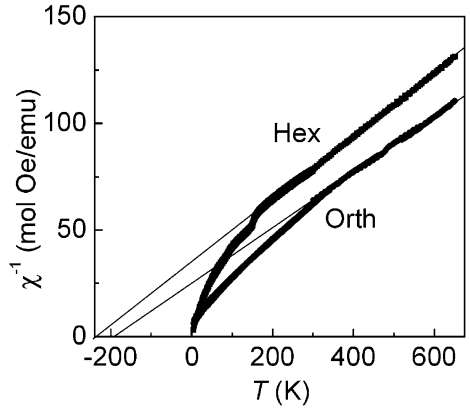

Figure 5. Reciprocal magnetic susceptibility (χ^{-1}) as a function of temperature for hexagonal (Hex) and orthorhombic (Orth) $YbMnO_3$.

phases, the high-temperature susceptibility obeys the Curie−Weiss law; that is, χ^{-1} exhibits a linear dependence on temperature above 160 K for h-$YbMnO_3$ and above 240 K for o-$YbMnO_3$. Fitting of the data to the equation $\chi_{exp} = C/(T - \theta)$ yielded the Weiss temperatures θ at −227 K and −189 K for the hexagonal and the orthorhombic phases, respectively, which is close to the reported value for h-$YbMnO_3$ (−200 K)[16] but notably lower than those for the

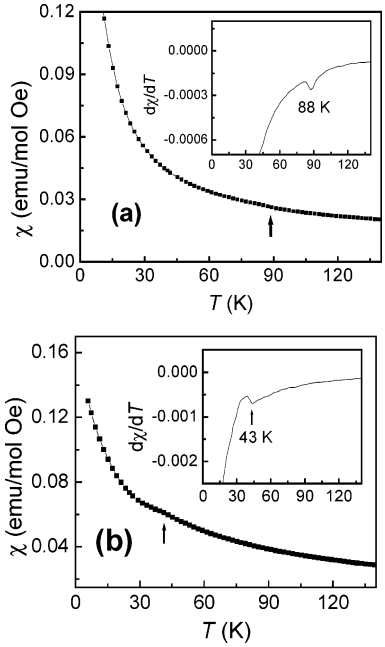

Figure 6. Temperature dependence of magnetic susceptibility (χ) at low temperatures under an external magnetic field of 100 Oe for (a) hexagonal and (b) orthorhombic $YbMnO_3$; the inset shows dχ/dT as a function of temperature.

other h-$RMnO_3$ compounds.[17−19] From the fitted value of the Curie constant C, effective paramagnetic moment values of $\mu_{eff} = 6.68$ and 6.37 μ_B were derived for h- and o-$YbMnO_3$, respectively. The theoretical paramagnetic moment is given by $\mu_{eff} = g_J[J(J + 1)])^{1/2}\mu_B$. For Mn^{3+} ions ($3d^4$, high-spin, $S = 2$, $g_J = 2$) the spin-only value is $\mu_{eff} = g_J[S(S + 1)])^{1/2}\mu_B = 4.90\ \mu_B$. For Yb^{3+} ions ($4f^{13}$, $S = 0.5$, $L = 3$, $J = 3.5$, $g_J = 1.143$), the theoretical value is $\mu_{eff} = 4.54\ \mu_B$. For the superimposed Mn^{3+} and Yb^{3+} sublattices in "$YbMnO_3$", one expects $\mu_{eff} = \sqrt{(\mu_{Mn}{}^2 + \mu_{Yb}{}^2)} = 6.68\ \mu_B$. This value concurs excellently with that observed for h-$YbMnO_3$ while being slightly higher than the observed value for o-$YbMnO_3$.

For both polymorphs, there is an anomaly in the susceptibility at low temperatures (see Figure 6) that signals a canted-spin AFM behavior. The thermal dependence of dχ/dT in the inset of Figure 6a shows an anomaly at 88 K for h-$YbMnO_3$, which is consistent with the reported Néel temperature ($T_N = 82$ K).[16] In h-$YbMnO_3$, the Mn^{3+} ion sits on a triangular sublattice for which AFM frustration favors a spin arrangement with neighboring spins rotated by 120° in the *ab* basal plane. For the orthorhombic phase, the dχ/dT curve exhibits a single anomaly at about 43 K (see Figure 6b), which corresponds well with the T_N for $YbMnO_3$ in Figure 1. As the R^{3+}-ion size decreases, the $MnO_{6/2}$ octahedra become more and more tilted, which lowers the σ-bond overlap integrals. However, Figure 1 shows that T_N only decreases with increasing tilt angle for the group I perovskites; it changes little among the group II perovskites. This

(16) Yoshii, K.; Abe, H. *J. Solid State Chem.* **2002**, *165*, 131.
(17) Huang, Z. J.; Cao, Y.; Sun, Y. Y.; Xue, Y. Y.; Chu, C. W. *Phys. Rev. B* **1997**, *56*, 2623.
(18) Katsufuji, T.; Mori, S.; Masaki, M.; Moritomo, Y.; Yamamoto, N.; Takagi, H. *Phys. Rev. B* **2001**, *64*, 104419.
(19) Muñoz, A.; Alonso, J. A.; Martínez-Lope, M. J.; Casáis, M. T.; Martínez, J. L.; Fernández-Díaz, M. T. *Phys. Rev. B* **2000**, *62*, 9498.

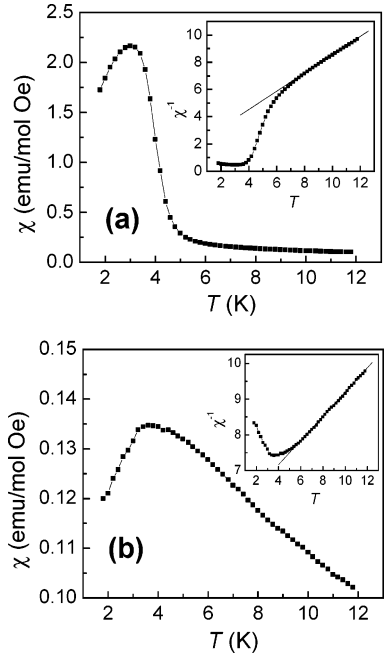

Figure 7. Temperature dependence of magnetic susceptibility (χ) in a very low-temperature region under an external magnetic field of 100 Oe for (a) hexagonal and (b) orthorhombic $YbMnO_3$; the inset shows χ^{-1} as a function of temperature.

observation shows that the strength of the spin−spin interatomic interactions is not controlled by the σ-bond overlap integrals alone. At lowest temperatures, the interaction between the Mn^{3+} and Yb^{3+} spins complicates the $M(T)$ behavior.[20] The low-temperature paramagnetic susceptibility measured under a field of 100 Oe is displayed in Figure 7. Both h- and o-$YbMnO_3$ exhibit an anomaly at about 4 K. The $\chi^{-1}(T)$ curves in the insets obey the Curie−Weiss law within certain temperature windows, that is, between 7 and 48 K for h-$YbMnO_3$ and between 6 and 30 K for o-$YbMnO_3$. Assuming a Curie−Weiss behavior, one derives $\mu_{eff} = 3.80$ μ_B and $\theta = -3.2$ K for h-$YbMnO_3$ and $\mu_{eff} = 4.83$ μ_B and $\theta = -16.4$ K for o-$YbMnO_3$. These numbers agree reasonably well with those expected for paramagnetic Yb^{3+}, that is, 4.54 μ_B. Hence, the magnetic anomaly at 4 K can be assigned to an ordering of the Yb^{3+} spins. A similar phenomenon at low temperatures was observed in both h- and o-$HoMnO_3$.[8]

The present NPD study shows a few additional diffraction peaks of magnetic origin at 9 K: the 001 peak is the most prominent. The observed magnetic peaks resemble those observed for $LaMnO_3$ with prominent (001) and (111) magnetic contributions[21] rather than the situation observed for o-$HoMnO_3$ with magnetic satellite reflections. As in $LaMnO_3$, the magnetic structure was found to be commensurate and of the A_y type with $\mu_{Mn} = 3.45(5)$ μ_B. No indication of Yb-sublattice ordering was observed at 9 K, in full accordance with the susceptibility data. An A_y type order in o-$YbMnO_3$ is unexpected. A return to type-A_y magnetic order as the R^{3+}-ion radius continues to decrease requires a more careful consideration of the factors that influence the strengths of the competitive spin−spin interactions. It is not predicted by the frustration model of Kimura et al.[7]

Conclusion

The orthorhombic $YbMnO_3$ perovskite was synthesized via a HP annealing technique. It represents a HP polymorph with respect to hexagonal $YbMnO_3$. Its crystal structure was established by Rietveld refinement of NPD data. The obtained lattice parameters (a, b, c), unit-cell volume (V), average bond lengths ⟨Mn−O⟩ and ⟨R−O⟩ for eight short bonds, and average bond angle ⟨Mn−O−Mn⟩ are consistent with trends expected on the basis of reports for less distorted rare-earth orthorhombic perovskites. By reducing the size of the rare-earth element from La to Yb, the average Mn−O−Mn angle decreases from 155 to 142° in the manganite structures, which results in severe tilts of the $MnO_{6/2}$ octahedra. Magnetization measurements show an AFM ordering of Mn^{3+} spins below $T_N = 43$ K and an effective paramagnetic moment μ_{eff} of 6.37 μ_B in the high-temperature range. At low temperatures, a magnetic ordering of the Yb^{3+} moments is observed at around 4 K. The long-range magnetic structure of $YbMnO_3$ at 9 K is apparently commensurate and A_y type. The factors determining the evolution of the relative strengths of the spin−spin interactions on the MnO_3 array need to be more carefully considered.

Acknowledgment. This work was supported by Grants-in-aid for Scientific Research (Nos. 15206002 and 15206071) from the Japan Society for the Promotion of Science. Y.H.H. acknowledges the Japan Society for the Promotion of Science (JSPS) for awarding him the Foreigner Postdoctoral Fellowship (ID P02315). H.F. acknowledges project support by the Research Council of Norway, Grant. 158518/431 (NANOMAT). J.B.G. thanks the Robert A. Welch Foundation, Houston, Texas, for financial support.

CM052758T

(20) Hemberger, J.; Brando, M.; Wehn, R.; Ivanov, V. Yu.; Mukhin, A. A.; Balbashov, A. M.; Loidl, A. *Phys. Rev. B* **2004**, *69*, 064418.

(21) Hauback, B. C.; Fjellvåg, H.; Sakai, N. *J. Solid State Chem.* **1996**, *124*, 43.